Single-Molecule Motility: Statistical Analysis and the Effects of Track Length on Quantification of Processive Motion

Andrew R. Thompson,* Gregory J. Hoeprich, and Christopher L. Berger
Department of Molecular Physiology and Biophysics, University of Vermont, Burlington, Vermont

ABSTRACT In vitro, single-molecule motility assays allow for the direct characterization of molecular motor properties including stepping velocity and characteristic run length. Although application of these techniques in vivo is feasible, the challenges involved in sample preparation, as well as the added complexity of the cell and its systems, result in a reduced ability to collect large datasets, as well as difficulty in simultaneous observation of the components of the motility system, namely motor and track. To address these challenges, we have developed simulations to characterize motility datasets as a function of sample size, processive run length of the motor, and distribution of track lengths. We introduce the use of a simple bootstrapping technique that allows for the quantification of measurement uncertainty and a Monte Carlo permutation resampling scheme for the measurement of statistical significance and the estimation of required sample size. In addition, we have found that, despite conventional wisdom, the measured characteristic run length is directly coupled to the characteristic track length that describes the microtubule length distribution. To be able to make comparisons between motility experiments performed on different track populations as well as make measurements of motility when motors and tracks cannot be simultaneously resolved, we have developed a theoretical framework for the determination of the effect that track length has on observed characteristic run lengths. This shows good agreement with in vitro motility experiments on two kinesin constructs walking on microtubule populations of different characteristic track lengths.

INTRODUCTION

In vitro characterization of motility from single-molecule processive motors such as kinesin-1, dynein, and myosin-V has led to a greater understanding of motor properties including stepping behavior (1), structure-function relationships (2,3), and regulation of motility by track-associated proteins (4–6) with an unprecedented level of precision. Furthermore, in vitro studies, whose components are comprised of isolated and expressed proteins, allow for ideal experimental conditions, as only the motor and track are variables in the system. This simplicity, though, comes with a significant departure from the physiological conditions that a motor protein experiences in the cell including a lack of molecular crowding and low ionic strength. Also, the lack of additional regulatory factors may mask how motors interact with their tracks within a cell. For example, early evidence in axons suggests that molecular trafficking may occur on dedicated microtubule tracks (7). Although the mechanisms behind this specification have yet to be elucidated, some potential avenues may be through the GTP hydrolysis state of tubulin (8), as well as the marking of tracks via posttranslational modifications, as acetylation and detyrosination have been implicated in promoting kinesin-1 binding and motility (9–12). Microtubule-associated proteins such as Tau may also play a role, as they have been shown to inhibit kinesin motility in vitro (4,6). Interestingly, similar levels of Tau inhibition have not been observed in the isolated axons of squid, which provides a more robust example of in vivo axonal conditions (13). Recent observations may yield a resolution to this paradox: inhibition of kinesin motility by Tau may be sensitive to the microtubule's nucleotide hydrolysis state, being inhibitory on GDP-like microtubules but not on GTP-like microtubules (5), which have been shown to be enriched in the axon (8). Such drastic discrepancies between in vitro and in vivo observations reveal a need for direct, single-molecule motor characterization in complete cell systems.

To accomplish this goal, in vivo single-molecule motility experiments can be performed through a variety of techniques to introduce fluorescently tagged motors in cells including pinocytosis (14,15), use of transfection reagents (16), and direct expression (9,17). Although these approaches directly address the physiological deficiencies of in vitro approaches, several new experimental challenges are evident including limited ability to introduce multiple fluorescent species and difficulty in the simultaneous observation of the motor and track due to cellular complexity, expression levels of the proteins of interest, and tradeoffs between signal/noise and rate of photobleaching (9,17). Whereas in vitro motility experiments are typically performed using total internal reflection fluorescence (TIRF) microscopy due to its superior signal/noise in single-molecule applications, its applicability to live-cell observation is limited to cell systems with flat morphologies whose motility components fall within the evanescent TIRF excitation field. As a consequence, epifluorescence is often employed, resulting in reduced signal/noise due to increased excitation of fluorophores in the bulk cytoplasm of the cell.

Submitted August 29, 2012, and accepted for publication May 8, 2013.

*Correspondence: thompsar@umn.edu

Editor: Claudia Veigel.

0006-3495/13/06/2651/11 $2.00

http://dx.doi.org/10.1016/j.bpj.2013.05.022

Perhaps the best illustration of the challenges faced by experimentation in vivo is found in the axon, whose small diameter (~1 μm for cultured mammalian axons (18)) and dense packing of microtubules limits the resolution of individual microtubules to techniques with high spatial resolution at the sacrifice of temporal resolution, such as superresolution fluorescence (8,19) or electron microscopy (20). As a result, characterization of motor behavior in an in vitro equivalent fashion is problematic, as the conventional motility protocol for the characterization of motility requires observation of the initial motor binding event, processive motion, and termination due to the motor unbinding from a continuous section of track. In the absence of simultaneous track observation, data may be contaminated with motility events that are artificially terminated by the track terminus which, intuitively, would result in the measurement of shorter characteristic run lengths. Moreover, the challenges present in sample preparation and observation may result in undersampling, leaving comparisons between experimental conditions in question.

In this article, we explore motility data in the context of processive kinesin movement on microtubule tracks, though the results and analysis techniques presented are applicable to other types of motility experiments both in vitro and in vivo. We examine common practices in motility data analysis and comparison and utilize simulations to demonstrate data behavior and sensitivity to sampling conditions. We demonstrate numerically derived criteria for the determination of adequate sampling and we propose a simple yet robust data-mining technique for the assessment of significance between data sets. Finally, to understand the effect on measured characteristic run length by datasets contaminated by microtubule-truncated motility, we have modeled motility collected with and without filtration of events experiencing artificial termination and have developed a theoretical framework for this effect. We demonstrate that measurements of characteristic run length are coupled directly to the underlying microtubule track distribution and are independent of whether or not motility reaching the end of the track is discounted. Thus, meaningful comparisons of motility data between experiments, whether performed in vitro or in vivo, can only be made when quantitatively accounting for the underlying microtubule distribution. These theoretical observations are supported with in vitro measurement of motility for two kinesin family members with different characteristic run lengths (kinesin-1 and kinesin-2) on microtubules with different length distributions, stabilized with guanosine-5-((α,β)-methyleno)triphosphate (GMPCPP), a slowly hydrolyzed GTP analog, or paclitaxel (Taxol).

MATERIALS AND METHODS

Simulations

All simulations were carried out using Mathematica Ver. 8 (Wolfram Research, Champaign, IL). Curve fitting was also performed in the software Mathematica using the FindFit function and default settings. Mathematica code for the various analysis techniques can be found in the Supporting Material.

In vitro motility

Microtubules stabilized with GMPCPP or Taxol were formed by mixing lyophilized rhodamine-labeled and unlabeled tubulin (Cytoskeleton, Denver, CO) at a 1:10 labeled/unlabeled ratio following previously reported methods (5). An eGFP-tagged kinesin-2 homodimer construct comprised of a C-terminal eGFP tag fused to a constitutively active (truncated at amino-acid 559) *Drosophila* kinesin-1 coiled-coil region with two KIF3A heads and their respective neck linkers as well as a similarly truncated eGFP *Drosophila* kinesin-1 construct were both generous gifts from Dr. William Hancock (Penn State University, State College, PA) (2).

The motility experiment was performed in motility buffer (10 mM PIPES, 50 mM potassium acetate, 4 mM magnesium acetate, 1 mM EGTA, pH 7.4 at 20°C) supplemented with 5.8 mg/mL glucose, 0.045 mg/mL catalase, and 0.067 mg/mL glucose oxidase to prevent photobleaching. Microtubule tracks were polymerized either in the presence of GTP followed by Taxol stabilization or GMPCPP and introduced into glass flow-chambers coated with anti-βIII-tubulin monoclonal antibodies (diluted to ~33 μg/mL in motility buffer from manufacturer's stock; Sigma-Aldrich, St. Louis, MO) and blocked with 1 mg/mL BSA in motility buffer. Experiments using sheared Taxol microtubules included 20 passages of the microtubules through a 25G needle immediately before introduction to the flow-chambers. The appropriate kinesin construct was then added at a concentration of 1nM in motility buffer with 1mM ATP. TIRF microscopy was performed at 20°C on an Eclipse Ti-U microscope (Nikon, Melville, NY) equipped with a PlanApo objective (100×, 1.49 N.A.). Movies were collected on an XR/Turbo-Z charge-coupled device camera (Stanford Photonics, Palo Alto, CA) at five frames/s with the exception of kinesin-2 GMPCPP data, which was collected at 3.33 frames/s. Motility was analyzed using the MTrackJ (21) plug-in for the software ImageJ (National Institutes of Health, Bethesda, MD) and track lengths were measured using the segmented line tool in ImageJ.

RESULTS AND DISCUSSION

Data behavior and convergence

Kinesin-1 walks on microtubules in a stochastic fashion, taking 8 nm hand-over-hand steps along a single microtubule protofilament (22,23). Observations of single molecules of kinesin have found the distribution of run lengths to be exponentially distributed (24,25). As such, the normalized probability density function $P(x)$ used to describe observed run lengths x of a population of motors is

$$P(x) = \frac{1}{x_0} e^{-\frac{x}{x_0}}, \quad (1)$$

where x_0 describes the characteristic processive run length of the motor population and, in the case of complete sampling along x, is equivalent to the expectation value $\langle x \rangle$. Conceptually, the representation of data as a histogram is clearest, as it directly sketches the probability distribution of motility outcomes. Another method of representation and analysis of run length data, though less common in the literature, is the plot of cumulative frequency $C(x)$,

$$C(x) = 1 - e^{-\frac{x-A}{x_0}}, \quad (2)$$

where A is an adjustment factor that accounts for undersampling of short runs. For example, we typically observe values of A in the range of 0.1–0.3 μm under our experimental conditions.

Utilizing this knowledge, we have simulated hypothetical motility datasets based on randomly sampling the probability distribution for a series of given characteristic run lengths within the range of values and sampling sizes reported in the literature. This is functionally equivalent to performing a motility experiment: we are sampling the population distribution of a sample, but here we know, a priori, the theoretical outcome given infinite sampling. The first observation is that measurements follow the central limit theorem: repeated sampling (i.e., repeat experiments) of the same population yield normally distributed characteristic run lengths with a standard deviation about the mean characteristic run length for repeated measurements decreasing proportional to the inverse of the square-root of the number of measurements (Fig. 1). This behavior also illustrates another important consideration: whereas standard experimental practice dictates repeat experiments, separate analysis, and a determination of mean value and spread, such a practice may be misleading in a measurement that is inherently a statistical sampling of a population distribution. In the presence of undersampling, uncertainty between measurements is not due necessarily to experimental variability, but can be due exclusively to fluctuations in sampling. The only solution, therefore, is to include all accumulated experimentally equivalent data in the analysis; systematic errors remain represented in the measured value whereas the uncertainty due to undersampling is minimized.

The next observation is that the standard deviation for repeated experiments with the same number of observations (N) increases as the characteristic run length increases (Fig. 2). On inspection, this behavior makes sense: given a histogram of run lengths and chosen bin width, the larger

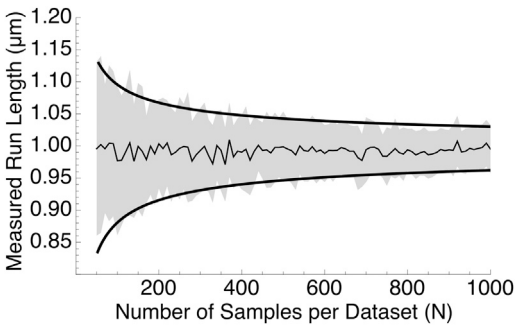

FIGURE 1 The effect of the number of samples per dataset (N) on a population of motors with a characteristic run length of 1 μm. The mean measured run length at a given N (*thin line*) was determined by performing 50 unique sampling experiments. The standard deviation about the mean (*shaded envelope*) fits well to a $N^{-1/2}$ relationship (*thick line*).

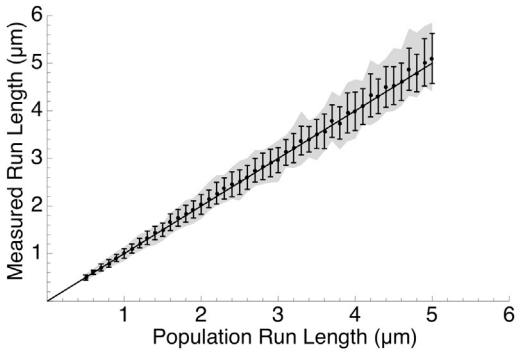

FIGURE 2 The standard deviation about the mean for repeat experiments (50 experiments, each with datasets of $N = 150$ points) increases as the characteristic run length of the population increases. The method of analysis also affects the standard deviation, with cumulative frequency analysis (*error bars*) having lower spread than the histogram analysis (*shaded envelope*). A line is drawn for the case of infinite sampling, where the measured run length equals the population run length. Both the mean determined via histogram analysis (not shown) and by cumulative frequency analysis (*points*) follow the expected behavior for infinite sampling.

the range of data, the more sensitive the fit to the distribution is to small fluctuations as it is not dominated by a few highly populated bins. Additionally, it also illustrates deficiencies in the analysis of data using the histogram representation as opposed to a cumulative frequency plot. Although both are technically equivalent representations, bin-width selection, whether assigned using experimentally determined criteria or using other binning criteria, tends to introduce higher deviation in measurement due to coarse-graining errors. As such, we favor cumulative frequency analysis in our fitting routines and use histograms merely for visualization purposes.

The behavior illustrated by Figs. 1 and 2 reveal the need to understand the adequacy of sampling present in the analysis. This is especially apropos when considering in vivo measurement, where accumulation of a large number of data points may be limited due to the experimental challenges not found in the equivalent in vitro experiment. Moreover, whereas increasing the sample size (N) always reduces the sampling error, the asymptotic $N^{-1/2}$ behavior of the uncertainty yields diminishing returns: the standard deviation in measurement of a characteristic run length of 1 μm with 150 data points is already within 5% of that of a dataset composed of 1000 data points (Fig. 1). Naturally, when performing a real experiment, such knowledge is hidden from us, requiring other means for deducing adequate sampling.

Additionally, the reporting of uncertainty in measurement and significance of measurement between observations has not been standardized in the motility field. As the probability distribution of runs is not normally distributed, values of standard deviation about the mean are not informative for characterizing data uncertainty. Although the sampling distribution of repeat measurements of the characteristic run

length is indeed normal (due to the central limit theorem), obtaining a representative distribution such that standard deviation about the mean becomes meaningful is experimentally impractical, especially when performing in vivo measurements. A common method for reporting uncertainty in measurement is a representation of the standard error of fit, but this value may give misleading confidence in the differences between populations.

These concerns, the quantification of uncertainty in measurement, the assessment of statistical significance between samples, and the amount of data needed to demonstrate significance, can be addressed by using simple bootstrap analysis techniques (26).

Bootstrap analysis of data uncertainty

To assess sampling uncertainty, we employed a simple bootstrap analysis of the dataset with the following procedure:

Bootstrap algorithm

Step 1. Resample the data, with replacement, N times, where N is equal to the length of the dataset.
Step 2. Perform a determination of characteristic run length of the resampled dataset.
Step 3. Repeat this resampling with sufficient repetition (~1000–10,000 times).
Step 4. Examine the resampling results with a histogram of measured characteristic run lengths.

The fundamental assumption when making a measurement—and repeat measurements to form a sampling distribution—is that our collected dataset is an accurate representation of the population. The bootstrapping procedure, therefore, assumes our data is a reasonable facsimile of the population and uses it to form a sampling distribution, thereby simulating the inherent propensity for fluctuation in the observed characteristic run length due to sampling statistics (26). The bootstrapped distribution cannot tell us any new information about the characteristic run length: the distribution will be centered near the dataset's measured value and its bias with respect to the population's actual characteristic run length will be maintained. The width of the distribution, though, is indicative of the error of measurement. Whereas the standard deviation of the bootstrap yields a parameter for measurement uncertainty (27,28), we prefer to measure 99% confidence intervals (~3 times the bootstrap standard deviation) as it offers a more coherent and generous representation of the uncertainty of measurement (Fig. 3). It should be noted that although common practice is to report standard error about the mean (mean $\pm$ SE), such a calculation should not be performed on the bootstrap distribution as it is proportional to the square-root of the number of bootstrap resamples.

Although the comparison between two datasets can be made by observing the overlap of their respective confidence intervals, this should be used in a qualitative sense and a more precise significance test is required. To assess statistical significance, as well as predict the amount of data required to determine statistical significance between two samples, we utilize a permutation resampling method that allows for a bootstrap-like approach for testing the null hypothesis.

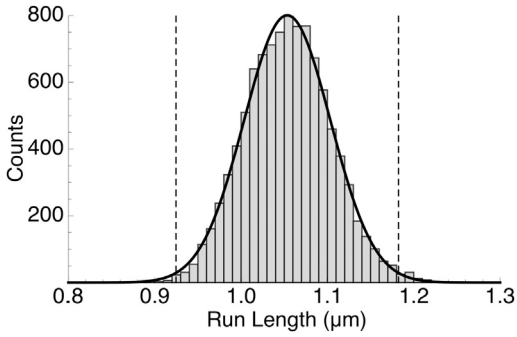

FIGURE 3 Bootstrap distribution for a measurement with 600 samples of a population of motors with a 1 μm characteristic run length. The distribution is well fit by a Gaussian, which is used to compute the 99% confidence intervals (*vertical dashed lines*).

Significance testing with permutation resampling

To assess statistical significance in the difference between two data sets of motility, we utilize a Monte Carlo permutation resampling scheme (26,29). This method has the direct advantage that the likelihood distribution of the null hypothesis—that the measured characteristic run lengths of each sample are identical—is directly generated from the data on hand rather than requiring a comparison with an idealized distribution. This method is robust as it is distribution-independent (i.e., nonparametric, unlike the Student's t-test), not affected by shape differences in each sample (e.g., skewness), and is not subject to the limitations and assumptions made by other nonparametric tests such as the Mann-Whitney test and is therefore less likely to report erroneous levels of significance (26). Despite its power, its use has been limited in the literature due to its computationally intense nature by the computing standards of the mid-late 20th century. With contemporary consumer-grade multicore processors and parallel processing, such computations can be performed in a matter of seconds.

Generation of the testing distribution begins with the selection of the test statistic of interest, in this case the difference between the measured characteristic run lengths of an experiment and control sample:

$$t_{\text{obs}} = x_{0\text{experiment}} - x_{0\text{control}}. \tag{3}$$

The null hypothesis follows, therefore, as

$$t_{\text{null}} = 0. \tag{4}$$

If the null hypothesis is applicable to our collected data, the labels of experiment and control on our respective datasets are meaningless; the data we have collected in each sample effectively comes from a sampling of the same population. By removing the labels on our data we can test such a scenario and generate a distribution of values of t_{null} (which should include zero) and observe the likelihood that t_{obs} is a member of t_{null}. If our data in each population are substantially different, the value of t_{obs} will fall well outside of the generated null datasets and can be ascribed a level of significance with the commonly used p-value notation (Fig. 4 *A*). To generate the null distribution:

Permutation resampling algorithm

Step 1. Note the size of each respective data pools ($N_{experiment}$, $N_{control}$).
Step 2. Mix data from experiment and control into a common pool.
Step 3. Generate two new datasets of size $N_{experiment}$ and $N_{control}$ by randomly sampling the common pool without replacement.
Step 4. Refit the newly formed datasets to acquire the characteristic run lengths.
Step 5. Measure and record the test statistic (t_{null}).
Step 6. Repeat Steps 1–5 with sufficient repetition (~1000–10,000 times).
Step 7. Plot the accumulated test statistics and compute appropriate confidence intervals (e.g., 99% intervals).
Step 8. Determine significance by comparison of t_{obs} with the t_{null} distribution confidence intervals.

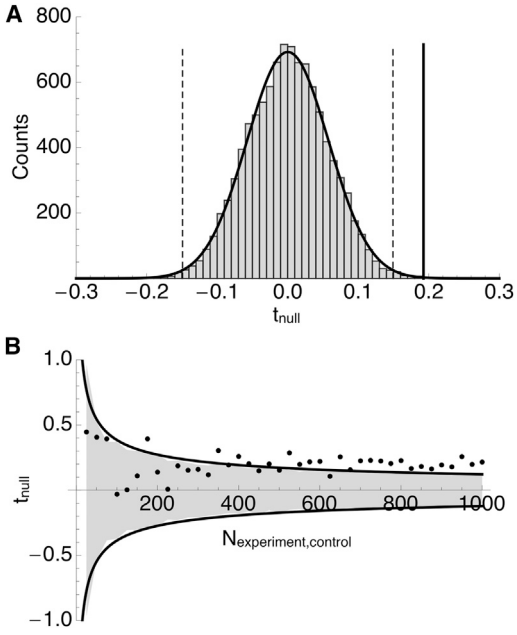

FIGURE 4 (*A*) A null hypothesis distribution generated by a permutation resampling of two samples of 600 points each measured from populations of motors with 1.0 μm and 0.8 μm characteristic run lengths. The observed difference (0.2 μm, *vertical line*) falls outside of the 99% confidence intervals, indicating a significant difference between the samples by our defined tolerance. (*B*) The 99% confidence intervals (*shaded envelope*) of the null hypothesis distribution for the populations in panel *A* as a function of data set size, which fits well to a $N^{-1/2}$ relationship (*thick line*). The observed difference between samples (t_{obs}, *points*) trends toward significant for $N_{experiment,control} \gtrsim 400$ as determined by Eq. 5.

In addition to the measurement of significance between experimental datasets, the permutation resampling scheme also allows for prediction of the necessary number of data points needed in each sampling to determine statistical significance given predicted values of $x_{0experiment}$, $x_{0control}$, and t_{obs}. Similar to the bootstrap distribution of a single run length measurement, the computed confidence intervals of the permutation resampling distribution decrease in a manner proportional to $N^{-1/2}_{experiment,\ control}$. Given hypothetical run lengths, $x_{0experiment}$ and $x_{0control}$, we have simulated datasets of equal size and computed the 99% confidence intervals of the resultant permutation distributions. By fitting these to a $N^{-1/2}_{experiment,\ control}$ distribution, we can determine the required number of data points $N_{experiment,control}$ to obtain a t_{obs} outside of the defined region of the null hypothesis rejection (Fig. 4 *B*). In the realm of reported kinesin processivity, the following approximation yields a reasonable estimate of required sampling to yield t_{obs} outside of the 99% confidence intervals of the null hypothesis distribution:

$$N_{experiment,control} \gtrsim \left(\frac{4x_{>}}{|t_{obs}|}\right)^2. \quad (5)$$

Here $x_{>}$ is the larger of $x_{0experiment}$, $x_{0control}$.

The effect of track length on observed motility

As discussed in the Introduction, accurate characterization of motor behavior leads one to examine motility within the cell to maintain physiological integrity. Although replication of the in vitro experimental system—where both motors and tracks are fluorescently tagged—is technically feasible, including expression of fluorescent proteins or post-motility antibody staining of tracks (9,17), these are challenging experiments that are not amenable to all cell types. Indeed, nowhere is this more evident than in the study of axonal transport, where axonal geometry and molecular crowding make simultaneous observation and colocalization of the motor and track, with both high spatial and temporal resolution, out of reach of contemporary methods.

Recall: Characterization of motility is accomplished by the repeat observation and tabulation of processive motility events where the motor can be seen to both bind and unbind from the microtubule track. Without simultaneous knowledge of the motor's position on the track, though, terminations of motility may be due to motors reaching the ends of tracks rather than due to their stochastic nature. The resulting data, therefore, will be artificially truncated and yield lower characteristic run lengths. A common

misconception is that by removing events that experience artificial truncation from the dataset, one measures the characteristic run length of the motors as if they were walking on tracks of infinite length.

We begin to test this assumption and quantify the effect of artificial termination with a theoretical framework, similar in approach to previous work examining the effect of track length on NTP turnover rates by nucleic acid motors (30). As demonstrated in Eq. 1, the quantity we are interested in measuring, the characteristic run length x_0, is merely the expectation value $\langle x\rangle_\infty$ of the run length probability distribution for the motors of interest on an infinite track. Given a track of finite length, we expect that a fraction of these motors—each expected to walk $\langle x\rangle_\infty$—would find themselves walking off of the end of the track and report a truncated run length. Thus, the observed behavior ($\langle x\rangle_{\text{obs}}$) to the experimenter who has no knowledge of the motor's position on the track will be

$$\langle x\rangle_{\text{obs}} = \langle x\rangle_\infty - \overline{q}\langle x\rangle_\infty, \tag{6}$$

where $\overline{q}$ is the average fraction of motors that have their motility truncated by the end of the track. On a given track of length L, each motor will land in a random position evenly distributed along its length, with a distance l of track remaining. Thus, for that specific track, the fraction of motors walking on it that have their motility truncated (q) is the ratio of the total probability of motors walking distances greater than the available track, divided by the total probability of all possible run lengths (i.e., the integral over all distances x of Eq. 1):

$$q = \frac{\int_l^\infty e^{-\frac{x}{x_0}}dx}{\int_0^\infty e^{-\frac{x}{x_0}}dx} = e^{-\frac{l}{x_0}}. \tag{7}$$

The average fraction of motors with truncated motility, $\overline{q}$, will be the average value of q over all possible landing sites on a single track (0 to L), weighted by the landing probability distribution for all possible track lengths $LT(L)/\alpha$,

$$\overline{q} = \int_0^\infty \left(\frac{1}{L}\int_0^L e^{-\frac{l}{x_0}}dl\right)\frac{LT(L)}{\alpha}dL, \tag{8}$$

where $T(L)$ is the measured track-length probability distribution function and α is the appropriate normalization factor for $LT(L)/\alpha$ as defined in Table S1 in the Supporting Material. Given stabilized microtubules grown in vitro tend to follow a Schulz distribution (31),

$$T(L) = e^{-\frac{L}{L_0}}\frac{L}{L_0^2}, \tag{9}$$

we arrive at an analytical solution for $\overline{q}$, and thus, after substitution of Eq. 8 into Eq. 6, $\langle x\rangle_{\text{obs}}$ as a function of the characteristic run length x_0 (i.e., $\langle x\rangle_\infty$) and the characteristic track-length L_0:

$$\langle x\rangle_{obs} = x_0\left(1 - \frac{x_0(L_0+2x_0)}{2(L_0+x_0)^2}\right). \tag{10}$$

To validate our theoretical framework, we simulated motility collected in a statistically distributed system of track lengths to compare the effect of artificial termination on the observed motility as compared to the motility observed on tracks of infinite length. The algorithm for this simulation is as follows:

Motility simulation algorithm

Step 1. Select a motility event from the motility probability distribution.
Step 2. Select a track from an appropriate microtubule landing probability distribution $LT(L)/\alpha$.
Step 3. Randomly choose a landing site along the selected microtubule.
Step 4. Compare the remaining track length available to the motor and adjust the length that the motor would be observed to walk if the motor's predestined run is longer than the available track.
Step 5. Repeat Steps 1–4 to generate a dataset of the desired size.
Step 6. Measure the resultant characteristic run length.

To fully observe the magnitude of motility truncation due to track distribution, we simulated motility events over a range of potential kinesin characteristic run lengths and microtubule populations obeying Schulz distributions. Under all values tested, we observed excellent agreement between theory and simulation (Fig. 5). As expected, motors selected from populations of low processivity (e.g., 0.4 μm characteristic run length) are little affected by artificial run length termination as compared to their expected behavior on infinite tracks. Substantial truncation occurs, though, for more processive motors such that motility of a single-motor type on different track-length distributions will report different levels of processivity when, in fact, the actual properties of the motor are unchanged.

Surprisingly, simulations where track-mediated terminations are eliminated from the final measurement of run length reveal behavior that is indistinguishable from that of motility where artificial terminations are left in the analysis. Reconsideration of the theoretical derivation reveals this should be expected behavior, though, as removal of data that is biased toward longer events as opposed to counting more short runs has the same functional effect, namely a reduction in the observed processivity. This observation has significant implications toward the analysis and comparison of motility data both in vitro and in vivo, as it reveals that the microtubule track distribution itself biases the observable motility events, in essence acting as a low-pass filter whose

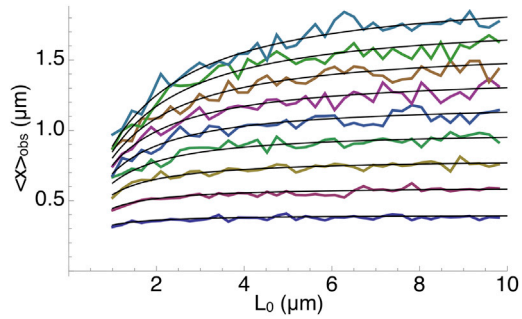

FIGURE 5 The effect of track length on measured run length ($\langle x \rangle_{obs}$), sampling populations of characteristic run lengths (x_0) from 0.4 μm to 2.0 μm in 0.2 μm steps with 1000 samples per dataset. Each population was subjected to tracks obeying Schulz distributions of various characteristic track lengths (L_0, Eq. 9). The theoretical derivation (Eq. 10, *lines*) shows excellent agreement with the simulation.

cutoff is set by the characteristic track length. More specifically, the characteristic run length measured in an experiment ($\langle x \rangle_{obs}$) is not, as often assumed, a direct measurement of the properties of the motor population alone (i.e., the characteristic run length of motors on infinite tracks). Instead, it depends on the underlying distribution of track lengths as well, as shorter tracks in the distribution can only support shorter motility events, thus biasing the overall motility distribution. Comparisons between experiments, therefore, can only be undertaken when the observations have been adjusted for microtubule filtration effects by measurement of the microtubule-length distribution and determination of $x_0 = \langle x \rangle_\infty$ via the theory presented above.

Whereas theory and experiment demonstrate that in vitro polymerized microtubules follow a Schulz distribution upon stabilization, other, more complicated distributions may apply in the face of shearing and annealing (31) or through variations in the microtubule polymerization protocol. In vivo, one can expect microtubule lengths to be substantially more complicated. Unlike in vitro microtubules, those found in vivo may only grow from one end of a nucleating seed, resulting in exponentially distributed lengths (31,32). Further confounding the situation are the cell's intrinsic regulatory factors for controlling microtubule length, such as the microtubule severing enzymes katanin, spastin, and fidgetin (33), which would further alter the microtubule length distribution.

Regardless of the physical and experimental mechanisms defining the microtubule distribution, to adjust our motility for track filtration we need only characterize the observed track distribution with a reasonable fit to a probability distribution. Upon determination of an acceptable distribution, filtered motility may be corrected by applying the ascertained microtubule distribution function to Eq. 8, which provides, in our testing, easily integrable solutions for exponential, Schulz, and mixed Schulz distributions, followed by substitution into Eq. 6 (see Table S1). Simulations utilizing populations composed of single Schulz distributions (as in Fig. 5), exponential distributions, or a linear combination of two Schulz distributions, all resulted in excellent agreement with the theoretical behavior.

As further proof of principle, we performed in vitro motility experiments on eGFP-tagged kinesin-1 (Kin-1) and kinesin-2 (Kin-2) constructs on microtubules grown in the presence of either GMPCPP, a slowly hydrolyzed GTP analog, or GTP followed by Taxol stabilization. In our experience, GMPCPP microtubule populations produce microtubule distributions with characteristic track lengths approximately twofold shorter than Taxol-stabilized microtubules, providing a good test bed for differences in track sizes. Motility was collected and analyzed for characteristic run length, including events that appeared to reach the end of the microtubule track ($\langle x \rangle_{obs}$, Table 1). Exclusion of events that appeared truncated by the track terminus from the analysis resulted in measured characteristic run lengths that showed no statistically significant difference (p-value $\geq$ 0.01, via permutation resampling) from the same dataset that included truncated events, as expected from our simulations. The motility data were then bootstrapped and fit to a Gaussian distribution to define an $\langle x \rangle_{obs}$ probability distribution as well as compute mean value and the 99% confidence intervals. Our measurements of $\langle x \rangle_{obs}$ for kinesin-1 and kinesin-2 on Taxol-stabilized microtubules are qualitatively consistent with previously published results using these constructs, with kinesin-1 being more processive than kinesin-2 (p-value $= 1 \times 10^{-4}$, Fig. 6 *B*, Table 1) (2). $\langle x \rangle_{obs}$ for kinesin-1 on GMPCPP microtubules was also consistent with previous results, being less processive than on Taxol-stabilized microtubules (p-value $= 2 \times 10^{-6}$) (5).

Track lengths were then measured and fit to a Schulz distribution (Figs. 6 *A*, and Eq. 9; and see Fig. S1 in the Supporting Material) to determine the characteristic track length (L_0). Whereas the measurements of track length in these experiments define an absolute measurement—the sampling distribution is the population distribution because

TABLE 1 In vitro motility of kinesin-1 and kinesin-2 on Taxol- and GMPCPP-stabilized microtubules

Sample	$\langle x \rangle_{obs}$	N_{points}	L_0[a]	N_{points}	x_0[b]
Kin-1 Taxol	1.31 ± 0.20	253	4.44 ± 0.83	178	1.57 ± 0.42
Kin-1 Taxol sheared	0.93 ± 0.11	348	2.03 ± 0.29	291	1.28 ± 0.30
Kin-1 GMPCPP	0.91 ± 0.11	301	2.48 ± 0.56	117	1.15 ± 0.28
Kin-2 Taxol	0.93 ± 0.14	275	4.48 ± 0.63	265	1.04 ± 0.26
Kin-2 GMPCPP	0.66 ± 0.08	567	2.13 ± 0.25	355	0.81 ± 0.16

All measurements are determined by Gaussian fits to their respective bootstrapped distributions and the values presented are the bootstrap center ± the 99% confidence intervals. The units of length are expressed in micrometers.

[a]Microtubule characteristic length (L_0) was determined by a fit to a Schulz distribution (Eq. 9) using cumulative frequency analysis (see Fig. S1).

[b]Determined via a Gaussian fit to the results of the x_0 computation algorithm.

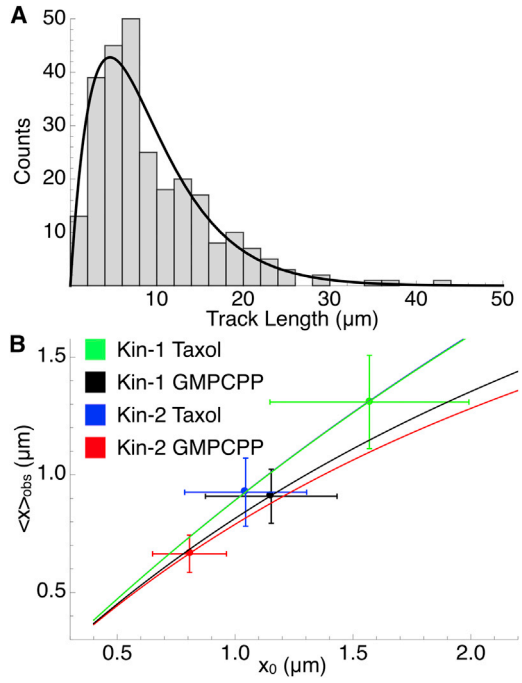

FIGURE 6 (*A*) A representative population of Taxol-stabilized microtubules fit to a Schulz length distribution ($L_0 = 4.59$ μm). (*B*) Correction of the experimentally derived motility ($\langle x \rangle_{obs}$, *y* axis) for track filtration effects to determine the actual characteristic run length (x_0, *x* axis) via utilization of Eq. 10 (*lines*) for Kin-1 on microtubules stabilized by Taxol and GMPCPP (*green* and *black*) and Kin-2 on similarly prepared tracks (*blue* and *red*). Data is represented by the mean value (*points*) and the 99% confidence intervals (*error bars*) of the computed run length bootstrap distributions. Values creating the x_0 distribution were determined by sampling all possible values of the $\langle x \rangle_{obs}$ bootstrap distribution as well as the microtubule-length (L_0) bootstrap distribution. Although only the mean value of the microtubule-length distribution is shown, the range of response curves for each condition is visualized in Fig. S2.

all microtubules are observed—we also bootstrapped the microtubule measurements to account for inadequacies of the fit to describe the actual microtubule distribution supporting motility (see Fig. S2). The probability distribution for the characteristic run length in the absence of track filtration, x_0, was determined via the following algorithm:

x_0 *Computation algorithm*

Step 1. Randomly select a value of $\langle x \rangle_{obs}$ from the motility bootstrap distribution.
Step 2. Randomly select a value of L_0 from the track bootstrap distribution.
Step 3. Compute x_0 via Eq. 10.
Step 4. Generate a dataset of equal size to the experimental dataset using x_0 as the population characteristic run length and analyze the dataset for characteristic run length.
Step 5. Bin the measured value and repeat Steps 1–4 with sufficient repetition (1000–10,000 times) to generate the x_0 probability distribution (see Fig. S3).

Calculations of the x_0 distribution for each respective dataset were well fit by a Gaussian distribution, which allowed for computation of the median x_0 as well as the 99% confidence intervals. Whereas the distributions exhibit signs of right skewness (whose population median was well aligned with the Gaussian center), we chose the Gaussian-derived parameters of center and confidence (as opposed to the direct computation of quantiles) purely to maintain symmetry for ease of presentation. Again, whereas the confidence intervals for x_0 are useful for visualization of the overlap between measurements, quantification of statistical significance must be achieved using a combination of the x_0 Computation Algorithm and the Permutation Resampling Algorithm, wherein Steps 1–4 of the x_0 Computation Algorithm are performed for each dataset, followed by computation of t_{obs} and *p*-value via the Permutation Resampling Algorithm. Iterated sufficiently (~1000 times), a maximum likelihood plot for t_{obs} and *p*-value may be generated (see Fig. S4 and Fig. S5).

Comparison of the simulated values of x_0 for kinesin-1 on Taxol and GMPCPP reveals a statistically significant difference between experiments (median *p*-value = 0.001, see Fig. S4), indicating a change in the fundamental processivity of the motor on GMPCPP microtubules and not merely an effect of the shorter tracks producing the observed differences in $\langle x \rangle_{obs}$ between samples. Kinesin-2 also showed a similar sensitivity to GMPCPP microtubules (median *p*-value = 0.001, see Fig. S5). To further verify kinesin-1's change in processivity on GMPCPP tracks, we performed measurements on Taxol microtubules that had been sheared to produce shorter tracks, which we hypothesized would not alter the fundamental processivity (x_0) of the motor. Shearing of microtubules by 20 passages through a 25G needle resulted in a population of tracks that was again well fit by a Schulz distribution ($L_0 = 2.03$ μm). Observed motility was shorter, consistent with the effect of track filtration, yielding an $\langle x \rangle_{obs}$ that is substantially different from that measured on the longer Taxol microtubules (*p*-value = 3×10^{-6}). Computation of x_0, though, reveals a characteristic run length that is statistically indistinguishable (median *p*-value = 0.03) from the measurement made on longer microtubules, despite the motility occurring on a microtubule population as short as that supporting the GMPCPP dataset (Fig. 7 *A*, and see Fig. S3 and Fig. S4). This observation is consistent with the hypothesis that kinesin-1 on Taxol-stabilized microtubules has the same fundamental characteristic run length regardless of the length distribution of the underlying microtubules. It also reveals that, without correcting motility for track filtration effects, erroneous significance would be ascribed to the following types of measurements: $\langle x \rangle_{obs}$ for kinesin-1 on GMPCPP and $\langle x \rangle_{obs}$ on sheared Taxol-stabilized microtubules show a statistically significant difference with respect to motility on the longer Taxol microtubules via their permutation resampling; however, only the GMPCPP data

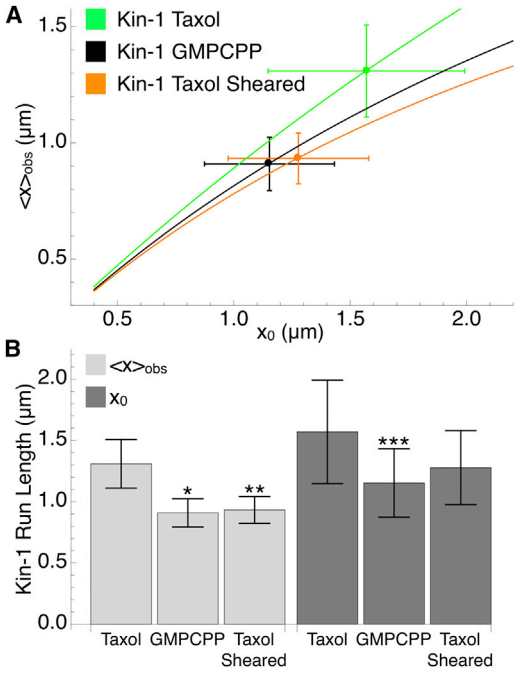

FIGURE 7 (*A*) Correction of the experimentally derived motility ($\langle x \rangle_{obs}$, *y* axis) for track filtration effects to determine the actual characteristic run length (x_0, *x* axis) via utilization of Eq. 10 (*lines*) for Kin-1 on microtubules stabilized by Taxol (*green*), GMPCPP (*black*), and sheared Taxol microtubules (*orange*). (*B*) Quantification of the statistical significance of Kin-1 motility on GMPCPP and sheared Taxol microtubules with respect to the Kin-1 motility measured on Taxol microtubules for the experimental ($\langle x \rangle_{obs}$, *light gray*) and corrected (x_0, *dark gray*) values for characteristic run length. Error bars signify the 99% confidence intervals. The presence of an asterisk signifies a statistically significant difference with *, **, and *** corresponding to *p*-values of 2×10^{-6}, 3×10^{-6}, and 0.001 (median), respectively, as computed by permutation resampling for $\langle x \rangle_{obs}$ comparisons and the generation of maximum likelihood plots for x_0 comparisons (see Fig. S4). The comparison of the corrected sheared Taxol motility with the corrected motility on long Taxol microtubules results in a median *p*-value = 0.03, which we consider to be a nonsignificant difference.

has distinguishable processivity from that on Taxol-stabilized microtubules upon quantification of x_0, when taking the underlying distribution of microtubule lengths into account (Fig. 7 *B*).

It is instructive to note that in the absence of our control of kinesin-1 motility on long, Taxol-stabilized microtubules, we would have made the incorrect conclusion that kinesin-1 has equivalent corrected processivity (x_0) on both GMPCPP and short Taxol-stabilized microtubules (median *p*-value = 0.18, Fig. 7 *B*, and see Fig. S4). Although the theory is nondegenerate—a given measurement of $\langle x \rangle_{obs}$ on a particular track distribution will yield a unique computation of x_0 for a noninfinite x_0—there are practical limitations to the applicability of the method (and the single-molecule motility assay) as dictated by not only our experimental resolving power but also our statistical resolution. This problem highlights the need for quantitative methods for the assessment of required data to make meaningful comparisons between motility datasets that, as discussed below, can be particularly limiting in the regime of short characteristic track lengths and long characteristic run lengths. The methods developed in this work, particularly Eq. 5, provide a framework to do so objectively.

As can be seen in Fig. 5, once values of x_0 are approximately half the characteristic track length, values of $\langle x \rangle_{obs}$ begin to converge, amplifying errors due to undersampling in the computation of x_0. In addition, as demonstrated in Fig. 2, for the same amount of data, uncertainty in run length measurement increases with increasing run length, thus increasing our uncertainty upon correcting for track effects. Together, these two behaviors result in a dramatic increase of the required data to demonstrate a statistically significant difference. Indeed, utilization of our rule-of-thumb estimate for the determination of required data (Eq. 5) reveals that we would need, at minimum, five times the data we are presenting to resolve a difference between the value for corrected kinesin-1 motility on sheared Taxol microtubules from the corrected motility for kinesin-1 on GMPCPP microtubules. As generating datasets of such size is not always experimentally practical, one should endeavor to make comparisons between motility datasets with the underlying track distributions as long as possible to make comparisons with reasonably sized datasets within reach. Also, where available, previous measurements of processivity should be used to guide experimental design choices when looking for functional effects based on changes in processivity. Though this behavior may limit the ability to make new conclusions based on corrected data, motility collected on distributions of tracks will always result in a foreshortening of the measured characteristic run length. To quantify differences between experiments in a meaningful and objective way, the techniques developed here must be applied to offset the effects of track-mediated biased sampling.

In in vitro experiments, where simultaneous observation of motor and track is typically trivial, care must be made to analyze the data in a statistically nonbiased fashion such that the data for motility and track length are collected independently. For example, correction of motility analyzed on only a single, long track should not be modified by the entire measured track distribution. In this extreme case, the effect can be easily determined by solving only the inner integral of Eq. 8—as $T(L)$ can be represented by the Dirac delta function centered on L—with the appropriate input of microtubule length. Measurement of motility on a single microtubule of 20 μm, for example, will result in $\langle x \rangle_{obs}$ being within 95% accurate when x_0 is 1 μm.

In the development of this methodology, our system of interest was the axon, whose microtubule lengths are quantifiable and exist in predominantly linear arrays (20). A quantitative application of this framework to other cell types is more limited in necessity and scope due to additional levels of cellular complexity. COS7 cells, for example,

show a complex meshwork of long microtubules—originating at the nucleus and extending to the cell periphery—with many points of potential intersection (9,34,35). Whereas our model implies motility on microtubules of such length would result in insignificant filtration of motility, examination of in vitro microtubule intersections has found that single molecules of kinesin may either ignore these junctions or be forced to dissociate (36). Motor type also plays a role in the importance of motility truncation. Kinesin-1 isoforms, for example, have been reported to preferentially bind and walk on stable, and thus predominantly longer microtubules (9,35). Kinesin-2 (KIF17), on the other hand, walks on both stable and dynamic microtubules and is therefore subject to more events reaching a microtubule terminus (9). Provided that the dynamic microtubules are not subject to external factors guiding their overall distribution, the methods we have demonstrated here are applicable.

One final consideration toward the applicability of this analysis technique in the collection and comparison of in vitro and in vivo motility is the presence and rate of photobleaching. Whereas the exact effects of photobleaching on observed motility are beyond the scope of this article, its presence will result in an apparent shortening of motility at higher rates of bleaching. To mitigate these effects, experiments in both in vitro and in vivo experimental regimes should be performed with equivalent rates of photobleaching and use constructs that are less susceptible to complete photobleaching (17).

SUMMARY

The characterization of motor protein properties in cells using the single-molecule motility assay faces several practical hurdles including limited ability to simultaneously resolve tracks and motors, increased complexity due to the protein dense cytoplasm, and reduced signal/noise due to observation limitations such as cell morphology, protein expression levels, and balancing fluorescence intensity with photobleaching (17). These limitations are particularly accentuated in the case of axonal transport, where observation of individual microtubule tracks is limited to the use of fixatives, electron microscopy, superresolution fluorescence techniques, or the use of model systems for axonal transport such as the extruded axoplasm of the squid *loligo pealei* (18). As a result, a careful understanding of the statistical limits of the measurement, as well as techniques for understanding the strength of the data when statistics are low or are affected by the lack of ability to simultaneously observe tracks and motors, is needed.

Utilizing simulation afforded by the existence of a theoretical and experimental basis of single-molecule motility behavior and readily available computing power, we have modeled motility in conditions likely to be experienced while performing motility experiments in the cell. By understanding the inherent fluctuations of a statistical sampling, we have developed criteria for representing measurement uncertainty by bootstrapping the acquired datasets to compute confidence intervals. Even in the cases of undersampling, we have demonstrated a Monte Carlo permutation resampling technique to measure the significance between datasets that avoids the need for assumptions inherent in other statistical tests and is therefore highly robust. Additionally, the permutation resampling technique allows for prediction of the amount of data required to demonstrate significance between the predicted observations. Finally, we observe that motility measured on populations of tracks is directly coupled to the track-length distribution, leaving uncorrected comparisons between datasets collected under different conditions in question. To adjust for this fact, we have simulated and developed a theoretical framework that, within the limits of statistical resolution, allows for the determination and correction of the effect of track-length distribution on observed motor processivity. With these tools we can make quantitative comparisons between different motility experiments performed in vitro, as well as comparisons between the motility observed in vitro with that collected in systems of increased complexity and in vivo.

SUPPORTING MATERIAL

One table and five figures are available at http://www.biophysj.org/biophysj/supplemental/S0006-3495(13)00578-X.

We thank Dr. William Hancock for the generous gift of the kinesin constructs. We also thank Dr. Andrej Vilfan, Dr. Jason Stumpff, and Dr. Derrick McVicker for helpful discussions during the preparation of this manuscript. Finally, we thank Dr. David M. Warshaw for microscope time and Guy Kennedy for operational support.

This work was supported by the National Institutes of Health (grant No. R21 NS066249 to C.L.B). A.R.T. was supported by National Institutes of Health's National Heart, Lung and Blood Institute postdoctoral fellowship (grant No. T32-HL007647).

REFERENCES

1. Warshaw, D. M., G. G. Kennedy, …, K. M. Trybus. 2005. Differential labeling of myosin V heads with quantum dots allows direct visualization of hand-over-hand processivity. *Biophys. J.* 88:L30–L32.
2. Shastry, S., and W. O. Hancock. 2010. Neck linker length determines the degree of processivity in kinesin-1 and kinesin-2 motors. *Curr. Biol.* 20:939–943.
3. Shastry, S., and W. O. Hancock. 2011. Interhead tension determines processivity across diverse N-terminal kinesins. *Proc. Natl. Acad. Sci. USA.* 108:16253–16258.
4. Dixit, R., J. L. Ross, …, E. L. Holzbaur. 2008. Differential regulation of dynein and kinesin motor proteins by Tau. *Science.* 319:1086–1089.
5. McVicker, D. P., L. R. Chrin, and C. L. Berger. 2011. The nucleotide-binding state of microtubules modulates kinesin processivity and the ability of Tau to inhibit kinesin-mediated transport. *J. Biol. Chem.* 286:42873–42880.
6. Vershinin, M., B. C. Carter, …, S. P. Gross. 2007. Multiple-motor based transport and its regulation by Tau. *Proc. Natl. Acad. Sci. USA.* 104:87–92.

7. Miller, R. H., R. J. Lasek, and M. J. Katz. 1987. Preferred microtubules for vesicle transport in lobster axons. *Science.* 235:220–222.
8. Nakata, T., S. Niwa, …, N. Hirokawa. 2011. Preferential binding of a kinesin-1 motor to GTP-tubulin-rich microtubules underlies polarized vesicle transport. *J. Cell Biol.* 194:245–255.
9. Cai, D., D. P. McEwen, …, K. J. Verhey. 2009. Single molecule imaging reveals differences in microtubule track selection between kinesin motors. *PLoS Biol.* 7:e1000216.
10. Reed, N. A., D. Cai, …, K. J. Verhey. 2006. Microtubule acetylation promotes kinesin-1 binding and transport. *Curr. Biol.* 16:2166–2172.
11. Konishi, Y., and M. Setou. 2009. Tubulin tyrosination navigates the kinesin-1 motor domain to axons. *Nat. Neurosci.* 12:559–567.
12. Hammond, J. W., C. F. Huang, …, K. J. Verhey. 2010. Posttranslational modifications of tubulin and the polarized transport of kinesin-1 in neurons. *Mol. Biol. Cell.* 21:572–583.
13. Morfini, G., G. Pigino, …, S. T. Brady. 2007. Tau binding to microtubules does not directly affect microtubule-based vesicle motility. *J. Neurosci. Res.* 85:2620–2630.
14. Courty, S., C. Luccardini, …, M. Dahan. 2006. Tracking individual kinesin motors in living cells using single quantum-dot imaging. *Nano Lett.* 6:1491–1495.
15. Nelson, S. R., M. Y. Ali, …, D. M. Warshaw. 2009. Random walk of processive, quantum dot-labeled myosin Va molecules within the actin cortex of COS-7 cells. *Biophys. J.* 97:509–518.
16. Yoo, J., T. Kambara, …, H. Higuchi. 2008. Intracellular imaging of targeted proteins labeled with quantum dots. *Exp. Cell Res.* 314:3563–3569.
17. Cai, D., K. J. Verhey, and E. Meyhöfer. 2007. Tracking single kinesin molecules in the cytoplasm of mammalian cells. *Biophys. J.* 92:4137–4144.
18. Brady, S. T., R. J. Lasek, and R. D. Allen. 1985. Video microscopy of fast axonal transport in extruded axoplasm: a new model for study of molecular mechanisms. *Cell Motil.* 5:81–101.
19. Gould, T. J., V. V. Verkhusha, and S. T. Hess. 2009. Imaging biological structures with fluorescence photoactivation localization microscopy. *Nat. Protoc.* 4:291–308.
20. Yu, W., and P. W. Baas. 1994. Changes in microtubule number and length during axon differentiation. *J. Neurosci.* 14:2818–2829.
21. Meijering, E., O. Dzyubachyk, and I. Smal. 2012. Methods for cell and particle tracking. *Methods Enzymol.* 504:183–200.
22. Vale, R. D., and R. A. Milligan. 2000. The way things move: looking under the hood of molecular motor proteins. *Science.* 288:88–95.
23. Yildiz, A., M. Tomishige, …, P. R. Selvin. 2004. Kinesin walks hand-over-hand. *Science.* 303:676–678.
24. Block, S. M., L. S. Goldstein, and B. J. Schnapp. 1990. Bead movement by single kinesin molecules studied with optical tweezers. *Nature.* 348:348–352.
25. Vale, R. D., T. Funatsu, …, T. Yanagida. 1996. Direct observation of single kinesin molecules moving along microtubules. *Nature.* 380:451–453.
26. McCabe, G. P., and D. S. Moore. 2006. Introduction to the Practice of Statistics. W. H. Freeman, New York.
27. Nagy, S., B. L. Ricca, …, R. S. Rock. 2008. A myosin motor that selects bundled actin for motility. *Proc. Natl. Acad. Sci. USA.* 105:9616–9620.
28. Walter, W. J., V. Beránek, …, S. Diez. 2012. Tubulin acetylation alone does not affect kinesin-1 velocity and run length in vitro. *PLoS ONE.* 7:e42218.
29. Good, P. I. 2000. Permutation Tests: a Practical Guide to Resampling Methods for Testing Hypotheses. Springer, New York.
30. Gyimesi, M., K. Sarlós, …, M. Kovács. 2010. Streamlined determination of processive run length and mechanochemical coupling of nucleic acid motor activities. *Nucleic Acids Res.* 38:e102.
31. Jeune-Smith, Y., and H. Hess. 2010. Engineering the length distribution of microtubules polymerized in vitro. *Soft Matter.* 8:1778–1784.
32. Dogterom, M., and S. Leibler. 1993. Physical aspects of the growth and regulation of microtubule structures. *Phys. Rev. Lett.* 70:1347–1350.
33. Sharp, D. J., and J. L. Ross. 2012. Microtubule-severing enzymes at the cutting edge. *J. Cell Sci.* 125:2561–2569.
34. Ross, J. L., M. Y. Ali, and D. M. Warshaw. 2008. Cargo transport: molecular motors navigate a complex cytoskeleton. *Curr. Opin. Cell Biol.* 20:41–47.
35. Dunn, S., E. E. Morrison, …, M. Peckham. 2008. Differential trafficking of Kif5c on tyrosinated and detyrosinated microtubules in live cells. *J. Cell Sci.* 121:1085–1095.
36. Ross, J. L., H. Shuman, …, Y. E. Goldman. 2008. Kinesin and dynein-dynactin at intersecting microtubules: motor density affects dynein function. *Biophys. J.* 94:3115–3125.